

A Detailed View of a Ribosomal Active Site: The Structure of the L11–RNA Complex

Brian T. Wimberly,* Rebecca Guymon,*
John P. McCutcheon,* Stephen W. White,†‡
and V. Ramakrishnan*‡

*Department of Biochemistry
University of Utah School of Medicine
Salt Lake City, Utah 84132

†Department of Structural Biology
St. Jude's Children's Research Hospital
and Department of Biochemistry
University of Tennessee
Memphis, Tennessee 38105

Summary

We report the crystal structure of a 58 nucleotide fragment of 23S ribosomal RNA bound to ribosomal protein L11. This highly conserved ribonucleoprotein domain is the target for the thiostrepton family of antibiotics that disrupt elongation factor function. The highly compact RNA has both familiar and novel structural motifs. While the C-terminal domain of L11 binds RNA tightly, the N-terminal domain makes only limited contacts with RNA and is proposed to function as a switch that reversibly associates with an adjacent region of RNA. The sites of mutations conferring resistance to thiostrepton and micrococin line a narrow cleft between the RNA and the N-terminal domain. These antibiotics are proposed to bind in this cleft, locking the putative switch and interfering with the function of elongation factors.

Introduction

The elongation cycle of protein synthesis is driven by two elongation factors that bind to nearly identical sites on the large (50S) ribosomal subunit (Spahn and Nierhaus, 1998; Wilson and Noller, 1998b). EF-Tu delivers aminoacyl tRNAs to the ribosome, whereas EF-G catalyzes the translocation of the ribosome by one codon relative to the mRNA and the concomitant movement of the A and P site tRNAs. Both elongation factors are G proteins, and their interactions with the ribosome are coupled to the binding and hydrolysis of GTP. Like most G proteins, EF-Tu and EF-G are molecular switches that have limited inherent GTPase activity, and they rely on an accessory factor to stimulate activity at the appropriate time. This accessory factor is an integral part of the 50S ribosomal subunit and has usually been referred to as the "GTPase center," but by analogy with the functionally equivalent GTPase-activating proteins that stimulate GTPase activity in G proteins, it seems more appropriate to refer to it as the "GTPase-associated region" (hereafter abbreviated as the GAR). Early work on the identification of the molecular components of the GAR implicated a complex between ribosomal protein L11

and a highly conserved 58 nucleotide stretch of 23S ribosomal RNA (rRNA), nucleotides 1051–1108 in *Escherichia coli* (Thompson et al., 1979; Schmidt et al., 1981). The L11–RNA complex is the target for a family of thiazole antibiotics that includes thiostrepton and micrococin. Thiostrepton binds essentially irreversibly to 50S subunits (Sopori and Lengyel, 1972) and inhibits hydrolysis of GTP by EF-G (Pestka, 1970), while micrococin binds to the same complex and stimulates GTP hydrolysis by EF-G (Cundliffe and Thompson, 1981).

Other components of the ribosome have also been implicated in stimulation of GTP hydrolysis by elongation factors. Classical work suggested that protein L7/L12, which together with L10 forms the "stalk" of the 50S subunit that lies adjacent to L11, is involved in stimulation of GTPase activity in EF-Tu (Donner et al., 1978). However, recently it has been shown that protein L7/L12, although essential for stalk formation, is not required for viability in yeast (Briones et al., 1998). The sarcin/ricin loop, a small, highly conserved stem-loop in the 23S rRNA that is known to be essential for ribosome function, has been footprinted by the elongation factors (Moazed et al., 1988) and is also considered a candidate for being part of the GAR. Recent kinetic experiments indicate that thiostrepton inhibits EF-G release rather than GTPase activity (W. Wintermeyer, personal communication), which suggests that the L11–RNA region does not directly stimulate GTPase activity. However, there is not yet a consensus on the precise functional role of the L11–RNA region, and in any event, it appears that this region plays some crucial GTPase-related role in translocation. For brevity, we continue to refer to the L11–RNA complex as the GAR.

The GAR is one of the most thoroughly characterized RNA–protein complexes. The secondary structure of the RNA was first inferred from biochemical and genetic studies (Glötz et al., 1981; Noller et al., 1981). It consists of a junction of four double-helical stems (Figure 1A). Approximately one-third of the residues in the GAR RNA are very highly conserved. The structure, thermodynamic stability, and ion-binding affinities of the RNA component have been extensively probed by a variety of biophysical and biochemical techniques; these data suggest that the 1067 and 1095 stem-loops are folded into a compact tertiary structure (Rosendahl and Douthwaite, 1994; Conn et al., 1998). Protein L11 consists of two domains: the C-terminal domain binds tightly to the RNA tertiary structure, while the N-terminal domain is required for the cooperative interaction with thiostrepton (Xing and Draper, 1996). The structure of the C-terminal domain has been determined by nuclear magnetic resonance (NMR) techniques (Hinck et al., 1997; Markus et al., 1997). Footprinting studies (Rosendahl and Douthwaite, 1993) have identified regions of RNA involved in the interaction with L11, while NMR chemical shift measurements (Hinck et al., 1997) have identified an RNA-binding surface on the C-terminal domain of the protein.

We present here the crystal structure of the ribosomal GAR from the hyperthermophilic eubacterium *Thermotoga maritima*. The structure explains most of the extensive

‡ To whom correspondence should be addressed (e-mail: stephen.white@stjude.org [S. W. W.], v.ramakrishnan@m.cc.utah.edu [V. R.]).

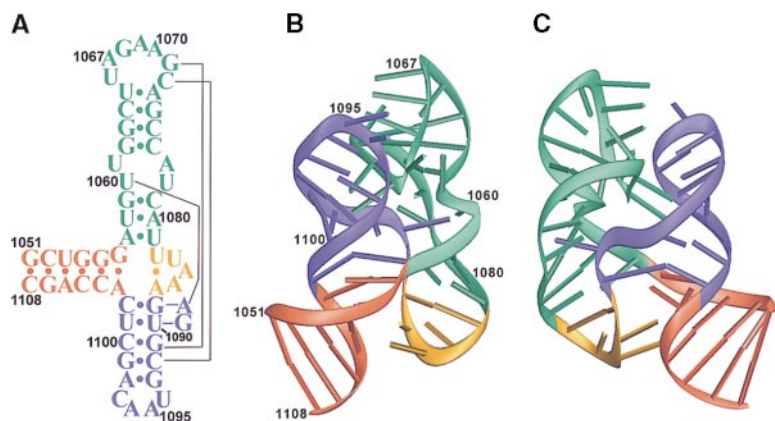


Figure 1. Overview of the Secondary and Tertiary Structure of the GTPase-Associated Region RNA from *Thermotoga maritima*

(A) RNA secondary structure derived from the crystal structure. Each of the four helical stems of the four-way junction is colored differently: red, the terminal stem; green, the 1067 stem-loop; gold, the 1082 hairpin; and blue, the 1095 stem-loop. Lines indicate long-range base triples and the long-range 1088–1060 base pair.

(B) Ribbon-and-stick schematic of the RNA tertiary structure, with the same color scheme used in (A). For clarity, protein L11 has been omitted from view.

(C) Same as (A), but the view is down the major groove of the 1095 stem to emphasize the compactness of the RNA fold. (B) and (C) were made with the program RIBBONS (Carson, 1991).

genetic and biochemical data available for this system, and it provides a framework for understanding the structural role played by the GAR in its interactions with elongation factors. The compact fold of the RNA component reveals new tertiary interactions that will help define the principles governing RNA folding. Finally, the structure is also potentially of great medical interest because it provides a new window on the mechanism of action of the thiostrepton family of antibiotics.

Results

The GAR RNA from the *T. maritima* 23S rRNA consists of nucleotides 1111–1168, which correspond to nucleotides 1051–1108 in the *E. coli* sequence. Hereafter, the *E. coli* numbering will be used in order to facilitate comparison with the available biochemical and genetic data. As described in the Experimental Procedures, we obtained crystals of the GAR RNA complexed with ribosomal protein L11 from *T. maritima* and solved the structure to 2.6 Å resolution using multiwavelength anomalous diffraction (MAD) on a mercury derivative of the crystal. Data collection, phasing, and refinement statistics are shown in Table 1. The asymmetric unit in the crystal consists of two 1:1 L11–RNA complexes stacked in a head-to-head manner. The two complexes are nearly identical except for a subtle bend in the terminal three base pairs of the RNA and a difference in the degree of disorder of the two L11 N-terminal domains. Several observations strongly suggest that the conformation observed in the crystal structure is extremely similar to the structure of the GAR in situ in the ribosome. The RNA contains all of the predicted secondary structure; the two complexes in the asymmetric unit are virtually identical; and, most significantly, the structure explains most of the large body of experimental data on this system.

Structure of the GAR RNA

The predicted secondary structure of the GAR RNA (Glötz et al., 1981; Noller et al., 1981) is almost identical to that derived from the crystal structure (Figure 1A). The RNA secondary structure contains four double-helical segments, referred to as the terminal stem (color coded

red in the figures), the 1067 stem-loop (green), the 1082 hairpin (gold), and the 1095 stem-loop (blue).

In the tertiary structure, the terminal stem stacks on the 1095 stem-loop and the 1067 stem-loop stacks on the 1082 hairpin. Thus, the four double-helical segments stack pairwise to form two extended helical subdomains. These two subdomains have irregular yet complementary shapes, so that the entire GAR RNA folds into a single compact globular domain (Figures 1B and 1C). The helical subdomains associate in a roughly parallel fashion, with the terminal stem packed against the 1082 hairpin and the 1067 and 1095 stem-loops packed against each other. Bulged-out residues in the 1067 and 1095 stem-loops mediate long-range tertiary interactions between the two subdomains. The fold requires two sharp turns in the backbone at the 1056–1057 and 1086–1087 phosphodiester linkages in the center of the junction, where the chain crosses over from one helical subdomain to the other. The molecule also contains a relatively large number of well-ordered metal ions that are integral to the structure.

A Ribose Zipper Joins the Terminal Stem and the 1082 Hairpin

The association of the terminal stem with the 1082 hairpin occurs via their minor grooves. This rather intimate packing is stabilized primarily by a dense network of hydrogen bonds between the riboses of nucleotides A1084–A1086 and C1104–A1106 (Figure 2A). A similar structural motif has been observed in the P4–P6 domain of the group I intron and has been referred to as a ribose zipper (Cate et al., 1996b). At the center of the four-way junction, the 2' OH of A1086 appears to be a particularly crucial component of the ribose zipper. It makes hydrogen bonds to A1103 N1 and G1056 2' OH and also directly ligates a crucial central cadmium ion (see below). A1086 has an unusual *syn* conformation that is necessary for the very tight packing of its sugar against the G1056–A1103 pair and for the reverse-Watson-Crick geometry of the U1082–A1086 pair (Figure 2C). Another noteworthy feature of the ribose zipper is a minor groove A-(G-C) triple involving nucleotides A1085, G1055, and C1104 (Figure 2C). This minor-groove triple has also

Table 1. Crystallographic Statistics

Data Collection			
	$\lambda 1$ (1.008 Å)	$\lambda 2$ (0.980 Å)	
Reflections	104,096	107,907	
Independent reflections	25,927	25,894	
Completeness	99% (98%) ^a	98% (97%) ^a	
Mean $[I/\sigma(I)]$	20 (4.2) ^a	20 (4.5) ^a	
R_{sym}	4.1% (17%) ^a	4.2% (17%) ^a	
d_{min} (Å)	2.6	2.6	
f' (Hg) (electrons) ^b	-12.0	-9.0	
f'' (Hg) (electrons) ^b	6.4	8.0	
f' (Cd) (electrons) ^b	-0.42	-0.46	
f'' (Cd) (electrons) ^b	2.3	2.2	
Phasing			
	$\lambda 1$ - $\lambda 2$ Isomorphous	$\lambda 1$ Anomalous	$\lambda 2$ Anomalous
R_{cullis} (centrics)	0.50	—	—
R_{Kraut} (acentrics)	0.09	0.025	0.023
Phasing power (acentrics)	1.25	1.54	1.52
Mean figure of merit (acentrics) 0.39			
Mean figure of merit (centrics) 0.23			
Refinement			
No. of atoms	4196 (2474 RNA, 1524 protein, 198 water and ions)		
$R_{\text{cryst}}/R_{\text{free}}$ (5% of data)	0.228/0.253		
Rms deviation from ideal geometry			
bond lengths	0.005 Å		
bond angles	1.1 degrees		

^a Values in parentheses refer to the highest resolution shell.
^b Values after SHARP refinement.

been found previously in large RNA tertiary folds (Cate et al., 1996b; Ferre-D'Amare et al., 1998).

Intimate Association of the 1067 and 1095 Stem-Loops by Reciprocal Donation of Bulges

The interaction between the 1067 and the 1095 stem-loops occurs primarily in their major grooves and is mediated largely by a reciprocal donation of highly conserved bulged-out bases. This unusually intimate major-groove packing is the primary reason for the compactness of the overall fold and it requires substantial distortions from regular helical geometry. This portion of the structure contains a large number of tertiary interactions, some of which are novel structural motifs.

The 1095 stem donates a bulged-out base, A1088, to a pocket created by a distortion in the 1067 stem (Figure 1). A1088 forms a universally conserved reverse-Hoogsteen pair with U1060 (Figure 2C). Because of steric constraints, A1088 must be in the *syn* conformation, which together with the reverse-Hoogsteen pairing geometry requires that U1060 must be flipped over. The inversion of U1060 is in turn facilitated by bulging out of the base of U1061. This inversion bulge, or S turn motif, has an S-shaped backbone conformation that has been observed previously (Szewczak et al., 1993; Wimberly et al., 1993; Wimberly, 1994). The insertion of A1088 also requires that residues A1077 and U1078 are unpaired and rotated out to open up the pocket. The unpaired conformation of these residues is stabilized by three hydrogen bonds to the sugar-phosphate backbone of the 1095 stem-loop at A1088 and G1089. Two

of these hydrogen bonds are to the base of A1077, which explains its universal conservation.

The reciprocal donation of a bulge from the 1067 stem-loop to the 1095 stem involves nucleotides G1071 and C1072, which form two novel long-range base triples with base pairs G1091-C1100 and C1092-G1099, respectively (Figures 2B and 2C). Within the 1095 stem-loop, nucleotides G1089-(U1090-U1101) also form a triple (Figure 2C), with G1089 acting as a stacking platform for the other two triples (Figure 2B). The stacking of G1071 on G1089 is further stabilized by hydrogen bonds between the 1089 2' OH and 1071 N3 and between the 1071 2' OH and the 1089 phosphate. These three base triples explain the sequence conservation of all these residues. The 1072-(1092-1099) triple was previously predicted and subsequently experimentally confirmed, although the geometry proposed for the triple (Conn et al., 1998) differs from that seen in the crystal structure.

The 1067 and 1095 Hairpin Loops

The highly conserved 1067 hairpin loop consists of two parts, a hairpin portion (U1066-A1069) that stacks on the sheared U1065-A1073 pair, and a three-nucleotide bulge (A1070-C1072) that participates in two different long-range tertiary interactions. The hairpin portion has a conformation commonly found in small hairpin loops with a U turn motif (Quigley and Rich, 1976) at U1066 and regular stacking of A1067-G1068-A1069. A1069 stacks on A1073, and its 2' OH hydrogen bonds to the N3 of U1065, thereby stabilizing the location of the 1069 sugar as well as the sheared geometry of the U1065-

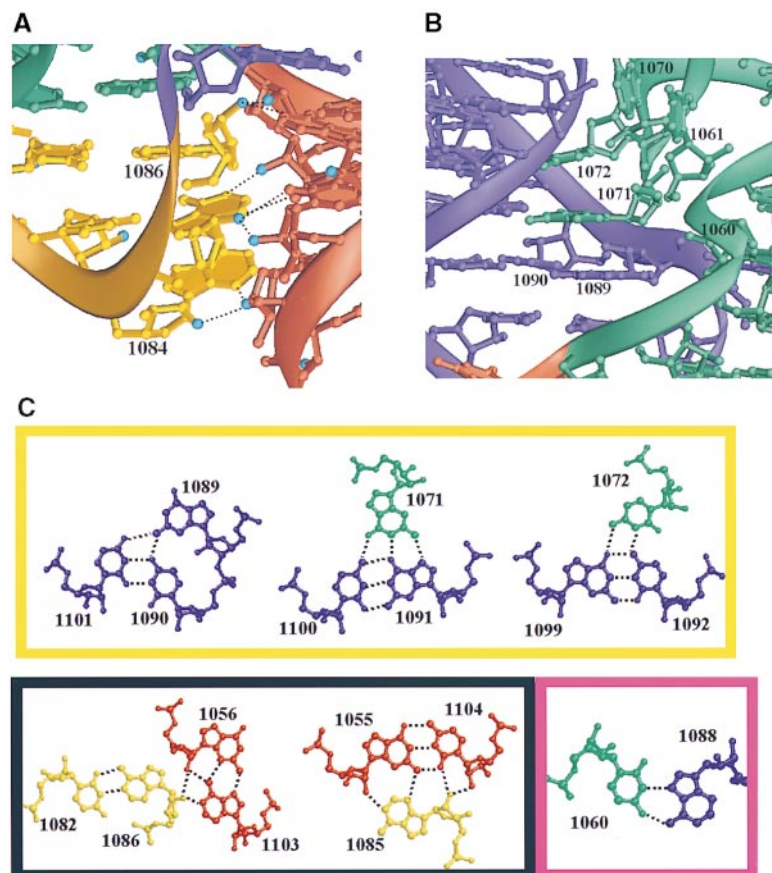


Figure 2. Selected Details of the Tertiary Structure of the GTPase-Associated Region RNA from *Thermotoga maritima*

The color coding corresponds to that described in Figure 1A. In (A) and (B), the RNA backbone is represented by a ribbon and the phosphates are not shown.

(A) The ribose zipper that mediates the minor-groove to minor-groove association of the terminal stem and the 1082 hairpin loop. The 2' oxygen of each sugar is highlighted in cyan. Hydrogen bonds are indicated by dotted lines.

(B) The major-groove to major-groove association of the 1067 and 1095 stem-loops, in a view emphasizing the high-five, S turn, and dinucleotide platform motifs. The high-five motif consists of the long-range stacking of two bulged residues, U1061 and A1070. The S turn comprises the inverted nucleotide U1060 and the bulged residue U1061. The dinucleotide platform motif consists of G1089 and U1090, on which the bulged residues G1071 and C1072 rest, as part of the long-range triples G1071-(G1091-C1100) and C1072-(C1092-G1099).

(C) Geometries of the noncanonical base pairs and base triples. Top, the three major-groove base triples in the core of the structure: G1089-(U1090-U1101), G1071-(G1091-C1100), and C1072-(C1092-G1099). Bottom left, the minor groove docking interactions (U1082-A1086)-(G1056-A1103) and A1085-(G1055-C1104). Bottom right, the long-range pair A1088-U1060. (A) and (B) were made with RIBBONS (Carson, 1991) and (C) with MOLSCRIPT (Kraulis, 1991).

A1073 pair. The three-nucleotide bulge has a corkscrew-like conformation in which A1070 is bulged to one side and G1071 and C1072 are bulged into the major groove of the 1095 stem-loop. A1070 makes a novel long-range stacking interaction with U1061 that we call a "high-five" motif (Figure 2B), while 1071 and 1072 participate in the long-range base triples described above. The high-five motif makes several hydrogen-bonding and van der Waals interactions with the 1095 hairpin loop, thereby stabilizing the relative orientations of the two hairpins.

The 1095 hairpin loop is also very highly conserved and has a regular conformation stabilized by a U turn at U1094 and a sheared G1093-A1098 pair. Part of the base of G1093 stacks over the base of C1072, so that the long-range base triples are tightly wedged between an overhang from the sheared G-A pair on one side and the G1089-(U1090-U1101) triple on the other side. The structure of the 1095 hairpin loop is very similar to an NMR-derived structure of a small stem-loop containing the same hairpin loop sequence (Fountain et al., 1996). The structural basis for the very high sequence conservation of several of the residues in the 1095 hairpin loop (i.e., A1095, A1096, and U/C1097) is not completely clear, but it may arise from interactions with the N-terminal domain of L11 (see below) or with other components of the ribosome.

Metal Ion Interactions with RNA

Three cadmium ions and at least seven magnesium ions are visible in the experimental electron density map.

One of the cadmium ions stabilizes the association of the two complexes in the asymmetric unit, but the other two are integral to the RNA structure, and these two sites are probably occupied by magnesium ions *in vivo*. Most of the ions mediate the close approach of phosphates in the interacting major grooves of the 1067 and 1095 stems, and five of these ions stabilize the location and conformation of the 1070-1072 bulge between the 1067 and 1095 stems (Figure 3A). A cadmium ion occupies a crucial location at the center of the four-way junction, where it makes either direct or water-mediated contacts with residues from all four double-helical stems (Figure 3B). This ion appears to stabilize both of the sharp turns at the center of the junction, that is, the 1056-1057 and 1086-1087 turns, and thereby plays an important role in determining the overall structure of the four-way junction.

The Structure of Ribosomal Protein L11

Ribosomal protein L11 consists of two globular domains connected by a linker region. The secondary structure and a sequence alignment of the protein are shown in Figure 4A, and the tertiary fold is shown in Figures 4B and 4C in the context of the complex. As described below, there is some flexibility between the two domains, but the linker is short and contains two conserved prolines (73 and 74) that provide inherent rigidity. Also, the domain interface consists primarily of conserved hydrophobic residues, notably Met-52, Ile-53, Pro-55, Pro-73, and Phe-77. These observations suggest that

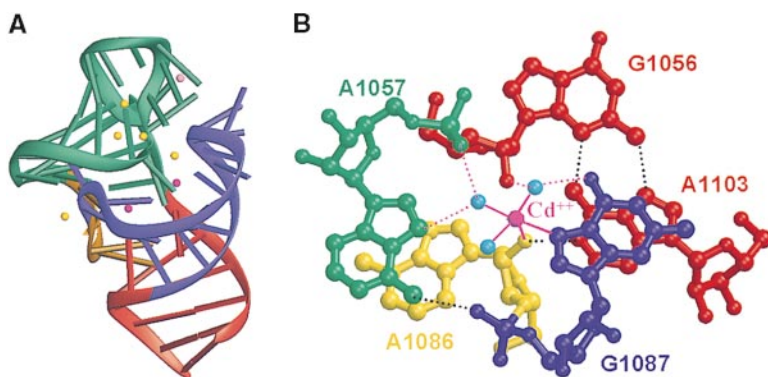


Figure 3. RNA-Metal Ion Interactions in the Tertiary Structure of the GTPase-Associated Region RNA from *Thermotoga maritima*

The color coding corresponds to that described in Figure 1A.

(A) Overview of the locations of the metal ions, showing that they are primarily in the interacting major grooves of the 1067 and 1095 stems. Magnesium ions are gold, cadmium ions are magenta, and the mercury ion is rose.

(B) Close-up of the central cadmium ion that stabilizes sharp turns at the 1056–1057 and 1086–1087 phosphodiester linkages at the center of the four-way junction. Direct ligation of the cadmium ion is indicated by solid magenta lines, and second-shell ligation is indicated by dotted magenta lines. (A) was made with RIBBONS (Carson, 1991) and (B) with MOLSCRIPT (Kraulis, 1991).

relative orientation of the two domains has not been greatly perturbed by crystal packing requirements.

The structure of the L11 N-terminal domain (NTD) consists of two helices packed against the concave surface of a three-stranded antiparallel β sheet, with an overall $\beta 1$ - $\alpha 1$ - $\alpha 2$ - $\beta 2$ - $\beta 3$ topology. The N-terminal seven residues are disordered. One of the most distinctive and conserved regions of the L11 molecule is the proline-rich helix 1, which appears to have a crucial functional role, as described below. The electron density for this helix was weak, and the register of the sequence in this helix may be in error by one residue. Indeed, the electron density for the entire NTD is rather poor, although of sufficient quality for an unambiguous determination of the fold. The average main chain B factor for the domain is 85 \AA^2 (for comparison, the average B factor of the C-terminal domain [CTD] is 40 \AA^2), indicating rigid body movement of the NTD within the crystal. This flexibility is consistent with the rather limited interactions seen between the NTD and other parts of the structure and may have functional implications (see below).

The structure of the CTD is in good agreement with the previously determined NMR structures of the CTD, both in isolation (Markus et al., 1997; Xing et al., 1997) and in the context of the L11-RNA complex (Hinck et al., 1997). The domain consists of a three-helical bundle and a short parallel two-stranded β -ribbon, with an overall $\alpha 3$ - $\beta 4$ - $\alpha 4$ - $\alpha 5$ - $\beta 5$ topology. All five secondary structure elements contribute to a conserved hydrophobic core. The domain is characterized by two extended loops that are disordered in the absence of the RNA but have defined structures in the complex.

The RNA-Protein Interaction

The two domains of L11 are very unequally associated with RNA. The CTD-RNA interface covers over 1700 \AA^2 of solvent-accessible surface area, while the NTD-RNA interface is less than 100 \AA^2 . This difference is consistent with the observation that the RNA-binding affinity of the CTD is essentially the same as that of the full-length protein (Xing and Draper, 1996).

The CTD binds the minor groove of the 1067 stem (Figures 4B and 4C), which is bent and flatter than the minor groove of a canonical A-form double helix. The RNA-binding surface of the CTD consists of one face

of helix 5, the N-terminal end of helix 3, and loops 6 and 7 that flank helix 5. Helix 5 is positioned lengthwise in the minor groove, and the flanking loops 6 and 7 extend this minor groove binding surface and also interact with the sugar-phosphate backbones on either side of the groove. A summary of the CTD-RNA interactions observed in the crystal structure (Figure 5A) emphasizes that the recognition of the RNA minor groove by L11 involves primarily interactions between the protein backbone and the RNA 2' OH moieties. Approximately half of the RNA-CTD hydrogen bonds involve a main chain amide or carbonyl, and over half of the 2' OH groups in the CTD footprint are hydrogen bonded to the protein. This preponderance of protein backbone-RNA backbone interactions indicates that overall shape complementarity between the RNA and protein must be an important determinant of specificity. Although binding appears to depend less on electrostatic interactions than on shape complementarity, there are a number of important salt bridges between basic side chains and phosphate groups: Lys-93, -126, and -133 and Arg-94 interact with one side of the minor groove and Lys-80, -87, and -112 with the other side. In the former group, the side chains are splayed away from protein, and the hydrophobic part of the side chain contributes to surface complementarity with the RNA. Side chains at the N terminus of $\alpha 5$ and within loop 7 make particularly intimate contact with the RNA, notably Ile-127 and Asn-117. Asn-117 points directly into the minor groove, making a number of hydrogen bonding interactions, and is one of the few side chains that formally "reads" the local RNA sequence. Two of the most important recognition elements in the RNA are the universally conserved long-range pair U1060-A1088 and the surrounding RNA internal loop that distorts to accommodate the insertion of A1088. Significantly, the RNA footprint of helix 5 encompasses this entire region of distorted RNA. The importance of the U1060-A1088 pair for L11 specificity is shown by the extremely high conservation of Gly-130 and Thr-131 to which these bases are hydrogen bonded (Figure 5B).

The NTD bridges the interface between the 1067 and 1095 stem-loops, and it makes only a few specific interactions with the RNA (Figure 4). Although its association with RNA is somewhat tenuous, which might be a result

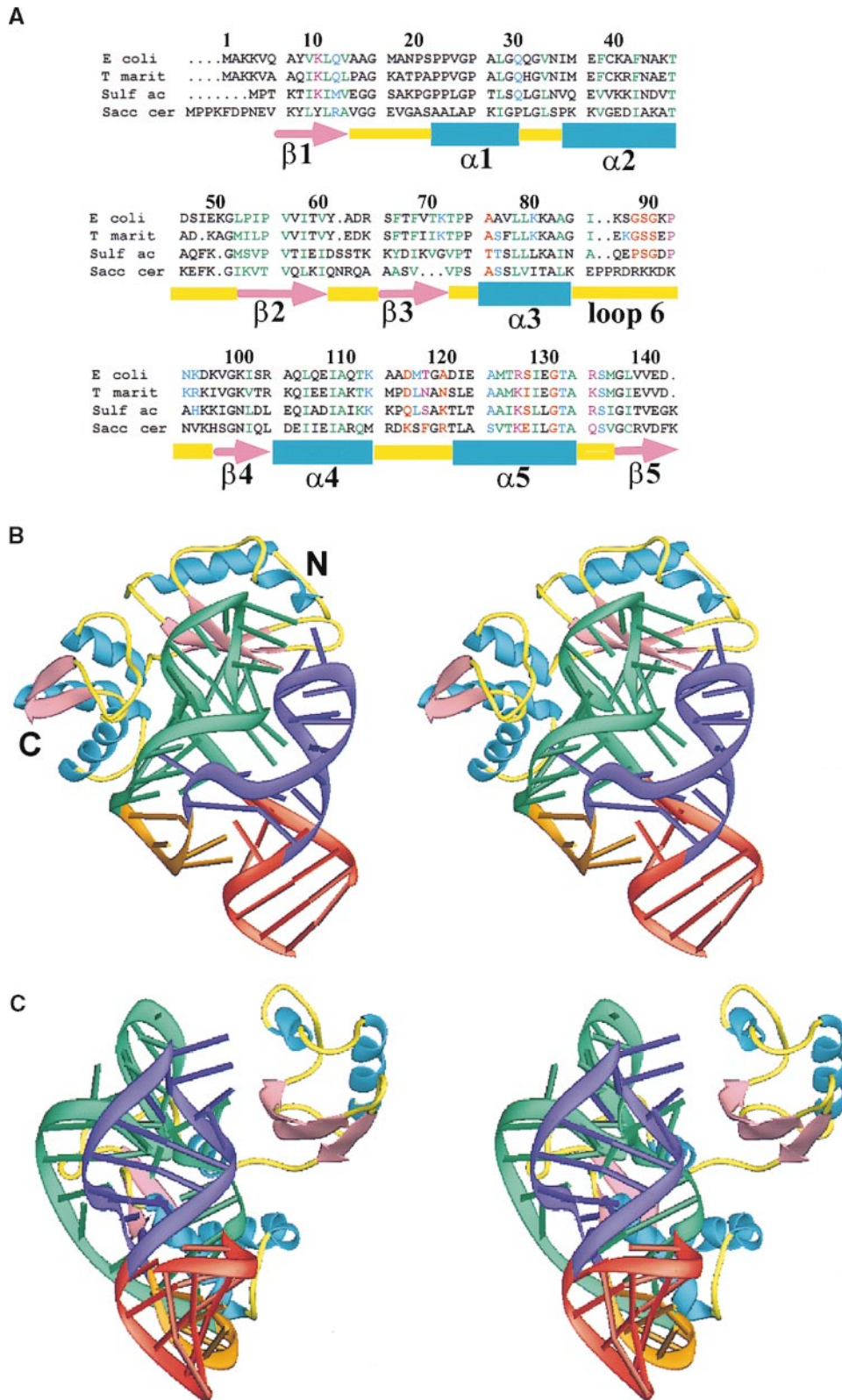


Figure 4. The RNA-L11 Complex within the GTPase-Associated Region from *Thermotoga maritima*

(A) Alignment of four widely divergent L11 sequences together with a schematic of the protein's secondary structure. The side chains of residues involved in the hydrophobic core in the crystal structure. Residues involved in RNA binding are colored blue for side chain contacts, red for main chain contacts, or purple if both the side chain and main chain interact with RNA. E. coli, *Escherichia coli*

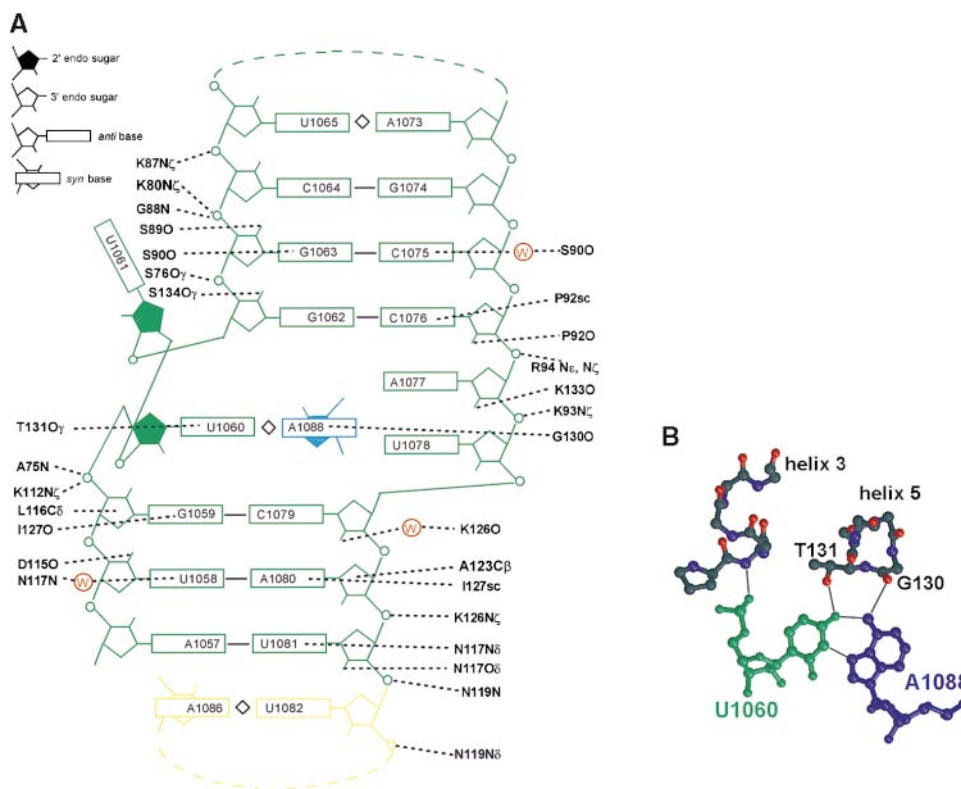


Figure 5. Protein-RNA Recognition within the GTPase-Associated Region from *Thermotoga maritima*

(A) Schematic of RNA-CTD interactions observed in the crystal structure. Unusual RNA conformational features are also indicated (see inset for key). The color coding is the same used in the other figures. Water molecules that mediate protein-RNA interactions are indicated in red. (B) Detail of the recognition of the conserved long-range A1088-U1060 pair by conserved L11 residues Gly-130 and Thr-131 from helix 5 and by the N terminus of helix 3. (B) was made with MOLSCRIPT (Kraulis, 1991).

of its binding mode having been altered by crystal packing requirements, the high sequence conservation of the NTD residues interacting with RNA suggests that the binding mode observed in the crystal structure is relevant to the structure of the complex in solution. Moreover, as described above, the structure of the NTD-CTD interface also suggests that the orientation of the NTD has not been greatly perturbed by crystal packing. The NTD residues interacting with RNA include Lys-10, Gln-12, Gln-30, and Lys-71. Lys-10 makes both main chain and side chain interactions with the RNA, and Gln-30 probably interacts specifically with A1095. There is also electron density interacting with the Watson-Crick face of C1097, but it is not clear whether this density arises from the NTD; examination of an anomalous difference Fourier map reveals that some of this density must correspond to a mercury or cadmium site. Finally, although the proline-rich sequence in helix 1 is surface exposed, highly conserved, and in the correct orientation for possible interactions with factors or antibiotics, it is close to but not in direct contact with RNA.

The Thiostrepton/Micrococcin-Binding Site

A1067 and A1095, at the ends of their respective stem-loops, have both been implicated in the binding of the antibiotics thiostrepton and micrococcin. Modification of A1067 by O2'-methylation (Cundliffe and Thompson, 1979; Thompson et al., 1982) or transversion mutations at either site (Rosendahl and Douthwaite, 1994) confers thiostrepton resistance. It has also been shown that thiostrepton affects the reactivity of both A1067 and A1095, suggesting that these two sites are close together (Rosendahl and Douthwaite, 1994), as indeed they are in the crystal structure. As for the role of L11 in antibiotic binding, it is known that L11 is required for high-affinity binding of thiostrepton to the RNA and that binding of L11 and thiostrepton to the RNA is cooperative. Thiostrepton has a much weaker affinity for the RNA alone ($K_d = 0.4 \mu\text{M}$), and it does not bind isolated L11 (Thompson et al., 1979). Two sites within the NTD of the protein have been implicated in this interaction: the mutations Pro22Ser and Pro22Thr confer thiostrepton resistance, while the antibiotic protects Tyr-61 (Tyr-

(eubacterium); *T. marit*, *Thermotoga maritima* (eubacterium); *Sulf ac*, *Sulfolobus acidocaldarius* (archaea); *Sacc cer*, *Saccharomyces cerevisiae* (eukaryote). The numbering is based on the *Thermotoga maritima* sequence present in the crystal structure.

(B) Stereo view of the complex. The L11 N- and C-terminal domains are labeled. The RNA is color coded as in Figure 1A. Note that the N-terminal domain straddles the interface of the 1067 (green) and 1095 (blue) stem-loops.

(C) Orthogonal stereo view of the complex. This view emphasizes the relatively loose association of the L11 N-terminal domain with the RNA. (B) and (C) were made with RIBBONS (Carson, 1991).

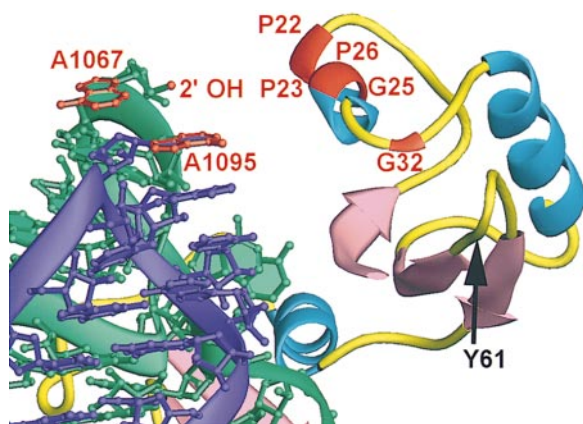


Figure 6. The Putative Thiostrepton/Micrococcin-Binding Site in the GTPase-Associated Region

The sites of mutations conferring resistance to thiostrepton and micrococcin are clustered around a cleft between the RNA and the proline-rich helix in the L11 N-terminal domain. Residues implicated in thiostrepton binding (A1067, A1095, and Pro-22) are highlighted in red and labeled. The position of Tyr-61, which is protected by thiostrepton in protein footprinting experiments, is also indicated. Other residues highlighted in red are those that confer micrococcin resistance (see text for details). The figure was made with RIBBONS (Carson, 1991).

62 in *E. coli*) in protein footprinting experiments (Porse et al., 1998). Recently, mutations that confer resistance to micrococcin have also been mapped to the NTD of L11 between residues 22 and 32 (Porse et al., 1999). All of these sites are located on a small surface of the NTD near A1067 and A1095 on the RNA (Figure 6). A prominent feature of this surface is the distinctive and highly conserved proline-rich helix, while Tyr-61 is over 20 Å distant. The clustering of these sites of antibiotic resistance mutations, together with the cooperative binding data, strongly suggests that the antibiotics bind to the cleft between the RNA and the proline-rich helix 1 of the NTD.

Discussion

The Structure of the RNA

Despite the accelerating pace of RNA structure determination, extremely little is known about RNA tertiary structure because only about five RNA folds have been determined. The crystal structure of the GAR RNA reveals an unexpectedly complex and compact fold that contains both well-known and novel structural motifs. The GAR RNA is in fact the most compact RNA structure yet reported, exposing only 138 Å² of solvent-accessible surface area per nucleotide (Nicholls et al., 1991). This extreme compactness is a result of extensive tertiary interactions along the entire length of the structure, in both the major and minor grooves. The other relatively compact known RNA folds exhibit primarily minor-groove packing (e.g., the P4–P6 domain of the group I intron) or primarily major-groove packing (e.g., tRNA) and are therefore less efficiently folded. It is probable that very efficient packing of RNA will be found to be common in the ribosome.

The crystal structure explains the molecular basis for

a number of important mutagenesis results. In particular, the RNA residues most sensitive to mutation are involved in tertiary interactions. For example, mutation of any of the universally conserved residues within the A1085–G1055–C1104 triple, a crucial part of the ribose zipper joining the terminal stem and the 1082 hairpin, dramatically destabilizes the RNA structure and greatly reduces the affinity for L11 (Lu and Draper, 1995). Mutation of C1072 to U within the 1072–(1092–1099) triple destroys the RNA tertiary structure, which demonstrates the energetic importance of this triple. Finally, the unusual observation that U1061A and U1061G mutants are more stable (Lu and Draper, 1994, 1995) is explained by the 1061–1070 high-five tertiary stacking motif, since purine stacking is more stable than pyrimidine stacking.

Stabilization of the RNA Tertiary Structure by Metal Ions

The crystal structure also reveals important new information about how metal ions interact with and stabilize unusual RNA structures. Biochemical experiments suggest that the GAR RNA contains high-affinity binding sites for two divalent cations (Bukhman and Draper, 1997) and one K⁺ or NH₄⁺ ion (Wang et al., 1993). The crystal structure reveals no fewer than seven magnesium sites and two cadmium sites, most of which stabilize the close approach of phosphates in the interacting major grooves of the 1067 and 1095 stem-loops. The metal ion stabilization of the 1070–1072 bulge conformation is qualitatively similar—though different in detail—to that seen in the A-rich bulge of the P4–P6 domain of the group I intron (Cate et al., 1996a). The striking structural role played by the central cadmium ion suggests that this site corresponds to one of the thermodynamically important ions. While more experiments will be necessary to test this hypothesis, it is worth noting that this cadmium ion is one of the two sites in the structure that ligates a guanosine N7. Both Mn²⁺ and Cd²⁺ preferentially bind to guanosine N7, and it has been observed that Mn²⁺ stabilizes the tertiary structure more than other divalent cations (Bukhman and Draper, 1997).

The Major-Groove Dinucleotide Platform: A Generalization of the Adenosine Platform

The crystal structure also reveals a new flavor of a known tertiary structure motif, the adenosine platform. In the structure of the P4–P6 domain, two successive adenines adopt a coplanar conformation—an adenosine platform—that serves as a stacking platform for a long-range tertiary interaction (Cate et al., 1996a). In the GAR structure, two successive nucleotides, G1089 and U1090, adopt the same conformation seen in the adenosine platform (Figure 2C). The two bases are coplanar, with a single N2–O4 hydrogen bond between them, and they also serve as a stacking platform for the 1071–1072 bulge involved in base triples (Figure 2B). There are, however, some differences between the GU platform seen here and the AA platform. In the P4–P6 structure, the motif is displayed in the minor groove rather than in the major groove, as is seen here. Moreover, in the P4–P6 structure it is the 3' adenosine upon which the long-range stacking interaction occurs, while here G1071 rests upon the 5' residue of the motif, G1089. Finally, the tertiary stacking

interaction occurs on opposite faces of the motif in the two structures. Despite these differences, the near identity of the conformations and functions of the motifs in these two structures leads us to suggest that the motif be referred to as a "dinucleotide platform," since it is clearly not restricted to adenosines. The few available data suggest that a GU dinucleotide platform may generally be more stable than an AA platform for major groove display. In the GAR, residues 1089 and 1090 are strictly conserved as either GU or AA, but mutation from AA to GU results in a significant stabilization of the RNA tertiary structure (Lu and Draper, 1994, 1995). The major-groove GU dinucleotide platform motif has also been found in small RNA structures lacking tertiary interactions (Szewczak et al., 1993; Wimberly et al., 1993), which suggests that in large structured RNAs, the GU dinucleotide platform may in some cases function as a preformed stacking platform supporting major-groove base triples.

Methylmercury as a Phasing Vehicle for RNA Crystal Structures

Surprisingly, the primary mercury site used in phasing is not near a cysteine of L11 but is located 2.4 Å from the N3 atom of U1061, consistent with a covalent mercury-uridine N3 bond. A similar, minor mercury site at U1078 is also visible in the anomalous difference Fourier map. Although most mercury adducts of pyrimidines have been obtained at the O4 or 5 positions of the base, a mercury 1-methylthymine adduct at N3 has been obtained at alkaline pH (Kosturko et al., 1974), and methylmercury salts have been shown to denature AT-rich DNA, consistent with reaction at thymine N3 (Gruenwedel and Davidson, 1966, 1967). Uracil is often preferred at bulge sites in RNA, so many larger RNA structures may contain solvent-accessible uracils. Therefore, methylmercury derivatization of RNA under native conditions, either prior or subsequent to crystallization, may be a generally useful method for obtaining heavy atom derivatives of RNA crystals without the laborious incorporation of sulfur-containing ribonucleotides.

The Structure of L11

The structure of the CTD was previously determined by NMR in both the free (Markus et al., 1997; Xing et al., 1997) and RNA-bound (Hinck et al., 1997) forms. Our crystal structure of the CTD is similar to that of the RNA-bound form determined by NMR, except for the conformation of the large RNA-binding loop 6 that is poorly determined in the NMR studies (Hinck et al., 1997). The mean C_{α} root-mean-square deviation (rmsd) for the crystal structure versus NMR ensemble is 2.7 Å overall, or 1.6 Å when residues 86–97 of loop 6 are excluded. For comparison, the mean rmsd within the ensemble of NMR structures is 2.3 Å for main chain atoms.

Many ribosomal proteins show structural similarities to families of DNA- and RNA-binding proteins (Ramakrishnan and White, 1998). It was noted from the NMR structure that the CTD of L11 has a homeodomain-like fold (Markus et al., 1997; Xing et al., 1997), and further NMR studies on the complex suggested that the CTD uses the typical homeodomain helix to bind RNA (Hinck et al., 1997). Although the crystal structure reveals that

this helix is indeed intimately associated with the RNA, its interaction does not bear any similarity to the base-specific recognition of a major groove by the homeodomains. Regarding the NTD, its overall $\alpha+\beta$ fold is similar to that seen in many other RNA-binding proteins (Ramakrishnan and White, 1998), but its $\beta-\alpha-\alpha-\beta-\beta$ topology has not yet been observed in an RNA-binding protein.

RNA-Protein Interaction

The L11-GAR RNA interaction has been probed by biochemical and NMR methods, and the crystal structure is in good agreement with the results of these studies, including a rather weak interaction between the RNA and the NTD. The RNA surface covered by the CTD corresponds fairly well to the residues protected by the binding of full-length L11, as shown by hydroxyl radical footprinting experiments (Rosendahl and Douthwaite, 1993). The RNA-binding surface of the CTD has been mapped by NMR chemical shift changes and relaxation studies (Hinck et al., 1997), and again the agreement with the crystal structure is excellent. The observation that L11 recognizes the RNA primarily by shape complementarity rather than by a side chain base reading of the RNA sequence is not surprising considering that the interaction occurs primarily via the minor groove. The interaction agrees with the prediction that relatively few highly conserved CTD residues would make specific side chain contacts with RNA (Xing et al., 1997). However, the related prediction that RNA binding by the CTD would not involve extensive recognition of the RNA bases is incorrect, as most of the base pairs are recognized by either hydrogen bonding or hydrophobic interactions. However, most of these hydrogen bonds occur via main chain amides or carbonyls rather than side chains. Finally, it is worth noting that L11 does not directly recognize the bulged-out nucleotides, which have previously been proposed as specificity determinants in ribosomal RNA-protein complexes.

Biochemical experiments have shown that L11 stabilizes the tertiary structure of the RNA and that this is a property of the CTD (Draper and Xing, 1995; Xing and Draper, 1995). Since nearly all of the direct RNA-protein contacts within the complex are to the 1067 stem, the resulting stabilization of the RNA tertiary structure appears to be indirect. The binding of one face of helix 5 with both strands of the 1067 stem is extensive and universally conserved, and this interaction must be particularly important for stabilization of the RNA tertiary structure. Consistent with a crucial role in RNA binding, helix 5 contains most of the mutation sites that have the greatest adverse effect on binding affinity (T131V, G130A, K126A, and S134A) (Xing et al., 1997). As for the RNA-binding loops 6 and 7, both are disordered when not bound to RNA (Markus et al., 1997), but they are highly ordered in the complex, and their conformations match the groove surface perfectly. The loops contain conserved structural features, which are important in the complex and may predispose them for RNA binding. Although it makes many interactions with RNA and contains the other two sites most sensitive to mutation (G88P and P92G), the longer RNA-binding loop 6 is relatively poorly conserved between kingdoms, with the bacterial and archaeal loops differing significantly from

the eukaryotic loops (Figure 4A). This variability in the protein sequence correlates with variability between phylogenetic kingdoms in the base pairing of the upper portion of the 1067 stem.

The NTD as a Molecular Switch

Prior to these structural studies, the molecular basis for cooperative binding within the RNA-L11-thiostrepton ternary complex was unknown. The crystal structure now provides a very straightforward explanation that also rationalizes the particular importance of the L11 NTD. The model also provides insights into how the GAR might function as a molecular switch.

The putative thiostrepton/micrococccin-binding site is centered on a small gap between helix 1 of the NTD and the 1067/1095 region of the RNA (Figure 6). The antibiotics are proposed to bind within this gap, possibly enlarging it somewhat, making specific interactions with the RNA on one side and further interactions with the NTD on the other side. In the absence of the NTD, the antibiotic's binding affinity would be greatly compromised, thus explaining the importance of the NTD for antibiotic binding (Xing and Draper, 1996). An alternative proposal, that thiostrepton binds directly only to the RNA and that this RNA conformation requires the presence of the NTD, is unlikely because the NTD does not appear to stabilize the RNA tertiary structure significantly and because the NTD sites of resistance mutations are not in contact with the RNA. In our model, the mechanism for the resistance to thiostrepton in Pro-22 mutants would be a disruption of direct thiostrepton-Pro22 interaction. A similar mechanism must hold true for the micrococccin sites given the more recent data (Porse et al., 1999). We also note that these antibiotics contain an array of thiazole rings that may mimic the array of prolines in the conserved proline-rich NTD helix.

How does thiostrepton inhibit EF-G function? An interesting speculation is that thiostrepton acts by trapping one of the many conformational states that must occur during elongation (Cundliffe, 1986). In their analysis of the effects of the Pro22Ser and Pro22Thr mutations, Porse et al. (1998) suggest that thiostrepton binding may affect the ability of the L11 NTD to undergo a conformational change, an idea that merits closer examination in light of the crystal structure. In the structure, the CTD is rather firmly anchored to one of the two RNA subdomains, while the NTD is somewhat tenuously bound across the RNA subdomain-subdomain interface. Even in the absence of other data, this overall architecture suggests that the NTD may function as a molecular switch that reversibly associates with the GAR RNA during the elongation cycle. In light of the other data—in particular the cooperative binding of thiostrepton and full-length L11 to RNA and the clustering of antibiotic resistance mutations to the cleft defined by A1067/A1095 and the proline-rich NTD helix—it appears even more likely that the NTD functions as a molecular switch and that the thiazole antibiotics work by binding to the NTD-RNA interface, thereby preventing the NTD from switching between RNA-bound and RNA-free states. It is likely that the switch is coupled to, or triggered by, the binding of elongation factors. Since L11 is not required for viability in *E. coli* (Stöffler et al., 1980), the switch

appears likely to function by controlling either the accessibility or the conformation of the GAR RNA.

This switch hypothesis could also explain why EF-Tu and IF2 do not footprint the 1067/1095 region of RNA while EF-G does, even though all these factors interact with the sarcin/ricin loop (Moazed et al., 1988). The sarcin/ricin loop is known to bind to a nearby (Wilson and Noller, 1998a) but distinct (Munishkin and Wool, 1997) site on EF-G. The EF-Tu-tRNA complex is similar in structure to EF-G, and the similarity is thought to be a case of molecular mimicry, with the factors binding to the same general region of the ribosome (Nissen et al., 1995). Thus, the footprinting differences could be explained if EF-Tu and IF2 recognize a different conformation of the switch than EF-G. This reasoning suggests that the two conformations of the GAR molecular switch correspond to different functional states of the ribosome.

Conclusions

This work provides a detailed view of a functionally important protein-RNA complex in the ribosome. The structure features a complex and very compact RNA fold stabilized by many bound metal ions, by a dense network of RNA tertiary interactions, and by extensive interactions with the protein. It also reveals novel principles of RNA folding, RNA-protein recognition, and indirect RNA tertiary structure stabilization. The structure provides a rationale for the large body of genetic and biochemical data on the GAR and a firm structural basis for future biochemical experiments on its function. The overall architecture of the complex suggests that the N-terminal domain functions as a molecular switch, either by facilitating changes in the tertiary structure of the GAR RNA or by controlling access to the RNA. Thiostrepton and micrococccin are proposed to bind to the NTD-RNA interface, thus locking the switch and disrupting factor function.

Experimental Procedures

Sample Preparation

The gene for *T. maritima* ribosomal protein L11 was cloned and overexpressed in *E. coli* using the T7-based expression system (Studier et al., 1990). The protein was purified by a combination of cation-exchange, hydroxylapatite, and size-exclusion chromatography as reported for the purification of ribosomal protein S7 (Wimberly et al., 1997). For cocrystallization with RNA, the protein was dialyzed into a buffer A containing 0.1 M KCl, 5 mM Na-cacodylate (pH 6.0), 0.1 mM Na₂EDTA, 1 mM DTT. A fragment of RNA corresponding to nucleotides 1111–1168 of *T. maritima* 23S rRNA was synthesized by in vitro run-off transcription from a linearized plasmid using T7 RNA polymerase. The plasmid contained the following elements: a T7 promoter, a self-cleaving hammerhead ribozyme to generate a homogeneous RNA 5' end (Price et al., 1995), a template for the target RNA sequence, and a PstI site used for plasmid linearization. RNA was purified on denaturing polyacrylamide slab gels, eluted, concentrated by ethanol precipitation, and dialyzed into buffer A. The RNA was annealed by heating to 90°C and slow cooling. L11 protein was added to yield a 1:1 RNA:protein mixture, which was concentrated to 0.15 mM in each component for crystallization experiments.

Crystallization and Structure Determination

Crystals of the complex were obtained at 4°C using the hanging drop technique. The equimolar mixture of L11 and RNA in dialysis buffer A was mixed with an equal volume of well solution (25%

glycerol, 15% PEG 4000, 0.2 M KCl, 50 mM MgCl₂, 20 mM CdCl₂, 1 mM DTT, 50 mM Tris [pH 7.5] at 22°C). The crystals were in the space group P2₁2₁2₁, with cell dimensions of $a = 63.9$ Å, $b = 84.3$ Å, and $c = 155.5$ Å, and diffracted to better than 2.6 Å resolution using a synchrotron source. Diffraction data were collected under cryogenic conditions, and the crystals were flash frozen by plunging into liquid nitrogen. For mercury derivatization, crystals were soaked for 24 hr in the well solution containing 1 mM CH₃HgNO₃, but lacking DTT. Efforts to obtain cocrystals of RNA with selenomethionine-substituted L11 were unsuccessful, apparently because our preparation of selenomethionyl L11 was at least partly misfolded.

The structure was solved using a MAD experiment (Hendrickson, 1991) on the methylmercury derivative. Straightforward isomorphous replacement was not possible because the derivative is not isomorphous with native crystals. Because the mercury LIII edge does not have a significant white line, data were collected at just two wavelengths, the inflection point of the mercury edge at 1.01 Å and a remote wavelength at 0.98 Å. This remote wavelength is near the maximum f'' for accurate measurement of anomalous differences and is also sufficiently remote from the inflection point to give useful isomorphous differences. Data were collected from a single flash-cooled crystal at beamline X12-C of the National Synchrotron Light Source (NSLS, Brookhaven National Laboratory). To optimize measurement of anomalous differences, we used the inverse beam method in which pairs of sweeps separated by 180 degrees were collected every 30 degrees. The data were integrated and scaled using the HKL suite of programs (Otwinowski and Minor, 1997).

Phasing was done by treating MAD as a special case of MIR (Ramakrishnan et al., 1993; Ramakrishnan and Biou, 1997). Local scaling of the data, determination of initial heavy atom sites, and initial phasing were done using the program SOLVE (Terwilliger and Berendzen, 1999). Subsequent phasing was done using the program SHARP (de la Fortelle and Bricogne, 1997). A significant improvement in phasing was obtained by including several well-ordered cadmium sites in a final round of SHARP heavy atom refinement. Each round of phasing was followed by density modification with SOLOMON (Abrahams and Leslie, 1996). The unaveraged, solvent-flattened map revealed virtually unbroken main chain density for the RNA and the L11 C-terminal domains of both complexes in the asymmetric unit, which were easily built using the program O (Jones and Kjeldgaard, 1997). Two-fold noncrystallographic symmetry (NCS) averaging followed by solvent flattening was then carried out using NCS and solvent masks based on the RNA and C-terminal domain coordinates. The resulting map was of high quality and revealed a few minor building errors, but the L11 N-terminal domain density was still of insufficient quality to permit unambiguous fitting. Interpretation of the density for the entire L11 N-terminal domain was possible only from iterative rounds of refinement and $2F_o - F_c$ maps. The final model was refined to an R_{free} of 25.4% using the program X-PLOR (Brünger, 1988) using standard parameters for protein (Engh and Huber, 1991) and nucleic acid (Parkinson et al., 1996) structure refinement. Magnesium and cadmium ions were distinguished by inspection of an anomalous difference Fourier map. Magnesium ions were distinguished from ordered waters by inspection of $2F_o - F_c$ maps, in which an octahedral coordination of magnesium by water and RNA ligands was often visible. A Ramachandran plot of the protein revealed only three outliers, Lys-93 in the C-terminal domain, which clearly has a positive phi angle in the original experimental map, and Thr-19 and Lys-64, which are in the generously allowed region and for which the side chains are very poorly defined. Details of the data collection, phasing, and refinement are shown in Table 1.

Acknowledgments

We thank R. M. Sweet and S. Sclafani for help with data collection on beamline X12C at the NSLS at Brookhaven National Laboratory; S. E. Gerchman for constructing the clone of L11 used in this study; Sandra Searles for the RNA transcription vectors pSS419 and pSS437; T. Terwilliger for advice with phasing using SOLVE; E. de la Fortelle for advice with phasing using SHARP; and J. P. Abrahams for advice with the use of input solvent masks in SOLOMON. This

work was supported by NIH grant GM 44973 (S. W. W. and V. R.). S. W. W. also acknowledges the continued support of the American Lebanese Syrian Associated Charities (ALSAC).

Received February 24, 1999; revised April 6, 1999.

References

- Abrahams, J.P., and Leslie, A.G.W. (1996). Methods used in the structure determination of bovine mitochondrial F1 ATPase. *Acta Crystallogr. D* 52, 30–42.
- Briones, E., Briones, C., Remacha, M., and Ballesta, J.P. (1998). The GTPase center protein L12 is required for correct ribosomal stalk assembly but not for *Saccharomyces cerevisiae* viability. *J. Biol. Chem.* 273, 31956–31961.
- Brünger, A.T. (1988). Crystallographic refinement by simulated annealing. Application to a 2.8 Å structure of aspartate aminotransferase. *J. Mol. Biol.* 203, 803–816.
- Bukhman, Y.V., and Draper, D.E. (1997). Affinities and selectivities of divalent cation binding sites within an RNA tertiary structure. *J. Mol. Biol.* 273, 1020–1031.
- Carson, M. (1991). Ribbons 2.0. *J. Appl. Crystallogr.* 24, 958–961.
- Cate, J.H., Gooding, A.R., Podell, E., Zhou, K., Golden, B.L., Szewczak, A.A., Kundrot, C.E., Cech, T.R., and Doudna, J.A. (1996a). RNA tertiary structure mediated by adenosine platforms. *Science* 273, 1696–1699.
- Cate, J.H., Gooding, A.R., Podell, E., Zhou, K., Golden, B.L., Kundrot, C.E., Cech, T.R., and Doudna, J.A. (1996b). Crystal structure of a group I ribozyme domain: principles of RNA packing. *Science* 273, 1678–1685.
- Conn, G.L., Gutell, R.R., and Draper, D.E. (1998). A functional ribosomal RNA tertiary structure involves a base triple interaction. *Biochemistry* 37, 11980–11988.
- Cundliffe, E. (1986). Involvement of specific portions of rRNA in defined ribosomal functions: a study utilizing antibiotics. In *Structure, Function and Genetics of Ribosomes*, B. Hardesty and G. Kramer, eds. (New York: Springer-Verlag), pp. 586–604.
- Cundliffe, E., and Thompson, J. (1979). Ribose methylation and resistance to thiostrepton. *Nature* 278, 859–861.
- Cundliffe, E., and Thompson, J. (1981). Concerning the mode of action of micrococin upon bacterial protein synthesis. *Eur. J. Biochem.* 118, 47–52.
- de la Fortelle, E., and Bricogne, G. (1997). Maximum-likelihood heavy-atom parameter refinement for multiple isomorphous replacement and multiwavelength anomalous diffraction methods. In *Methods in Enzymology*, C.W. Carter, Jr. and R.M. Sweet, eds. (New York: Academic Press), pp. 472–493.
- Donner, D., Villems, R., Liljas, A., and Kurland, C.G. (1978). Guanosinetriphosphatase activity dependent on elongation factor Tu and ribosomal protein L7/L12. *Proc. Natl. Acad. Sci. USA* 75, 3192–3195.
- Draper, D.E., and Xing, Y. (1995). Protein recognition of a ribosomal RNA tertiary structure. *Nucleic Acids Symp. Ser.* 33, 5–7.
- Engh, R.A., and Huber, R. (1991). Accurate bond and angle parameters for x-ray protein structure refinement. *Acta Crystallogr. A* 47, 392–400.
- Ferre-D'Amare, A.R., Zhou, K., and Doudna, J.A. (1998). Crystal structure of a hepatitis delta virus ribozyme. *Nature* 395, 567–574.
- Fountain, M.A., Serra, M.J., Krugh, T.R., and Turner, D.H. (1996). Structural features of a six-nucleotide RNA hairpin loop found in ribosomal RNA. *Biochemistry* 35, 6539–6548.
- Glötz, C., Zwieb, C., Brimacombe, R., Edwards, K., and Kössel, H. (1981). Secondary structure of the large subunit ribosomal RNA from *Escherichia coli*, *Zea mays* chloroplast, and human and mouse mitochondrial ribosomes. *Nucleic Acids Res.* 9, 3287–3306.
- Gruenwedel, D.W., and Davidson, N. (1966). Complexing and denaturation of DNA by methylmercuric hydroxide. I. Spectrophotometric studies. *J. Mol. Biol.* 21, 129–144.
- Gruenwedel, D.W., and Davidson, N. (1967). Complexing and denaturation of DNA by methylmercuric hydroxide. II. Ultracentrifugation studies. *Biopolymers* 5, 847–861.

- Hendrickson, W.A. (1991). Determination of macromolecular structures from anomalous diffraction of synchrotron radiation. *Science* 254, 51–58.
- Hinck, A.P., Markus, M.A., Huang, S., Grzesiek, S., Kustonovich, I., Draper, D.E., and Torchia, D.A. (1997). The RNA binding domain of ribosomal protein L11: three-dimensional structure of the RNA-bound form of the protein and its interaction with 23 S rRNA. *J. Mol. Biol.* 274, 101–113.
- Jones, T.A., and Kjeldgaard, M. (1997). Electron-density map interpretation. *Methods Enzymol.* 277B, 173–207.
- Kosturko, L.D., Folzer, C., and Stewart, R.F. (1974). The crystal and molecular structure of a 2:1 complex of 1-methylthymine-mercury (II). *Biochemistry* 13, 3949–3952.
- Kraulis, P. (1991). MOLSCRIPT: a program to produce both detailed and schematic plots of protein structures. *J. Appl. Crystallogr.* 24, 946–950.
- Lu, M., and Draper, D.E. (1994). Bases defining an ammonium and magnesium ion-dependent tertiary structure within the large subunit ribosomal RNA. *J. Mol. Biol.* 244, 572–585.
- Lu, M., and Draper, D.E. (1995). On the role of rRNA tertiary structure in recognition of ribosomal protein L11 and thiostrepton. *Nucleic Acids Res.* 23, 3426–3433.
- Markus, M.A., Hinck, A.P., Huang, S., Draper, D.E., and Torchia, D.A. (1997). High resolution solution structure of ribosomal protein L11-C76, a helical protein with a flexible loop that becomes structured upon binding to RNA. *Nat. Struct. Biol.* 4, 70–77.
- Moazed, D., Robertson, J.M., and Noller, H.F. (1988). Interaction of elongation factors EF-G and EF-Tu with a conserved loop in 23S RNA. *Nature* 334, 362–364.
- Munishkin, A., and Wool, I.G. (1997). The ribosome-in-pieces: binding of elongation factor EF-G to oligoribonucleotides that mimic the sarcin/ricin and thiostrepton domains of 23S ribosomal RNA. *Proc. Natl. Acad. Sci. USA* 94, 12280–12284.
- Nicholls, A., Sharp, K.A., and Honig, B. (1991). Protein folding and association: insights from the interfacial and thermodynamic properties of hydrocarbons. *Proteins* 11, 281–296.
- Nissen, P., Kjeldgaard, M., Thirup, S., Polekhina, G., Reshetnikova, L., Clark, B.F., and Nyborg, J. (1995). Crystal structure of the ternary complex of Phe-tRNA^{Phe}, EF-Tu, and a GTP analog. *Science* 270, 1464–1472.
- Noller, H.F., Kop, J., Wheaton, V., Brosius, J., Gutell, R.R., Kopylov, A.M., Dohme, F., Herr, W., Stahl, D.A., Gupta, R., and Woese, C.R. (1981). Secondary structure model for 23S ribosomal RNA. *Nucleic Acids Res.* 9, 6167–6189.
- Otwinowski, Z., and Minor, W. (1997). Processing of x-ray diffraction data collected in oscillation mode. *Methods Enzymol.* 276, 307–325.
- Parkinson, G., Vojtechovsky, J., Clowney, L., Brünger, A.T., and Berman, H.M. (1996). New parameters for the refinement of nucleic acid containing structures. *Acta Crystallogr. D* 52, 57–64.
- Pestka, S. (1970). Thiostrepton: a ribosomal inhibitor of translocation. *Biochem. Biophys. Res. Commun.* 40, 667–674.
- Porse, B.T., Leviev, I., Mankin, A.S., and Garrett, R.A. (1998). The antibiotic thiostrepton inhibits a functional transition within protein L11 at the ribosomal GTPase centre. *J. Mol. Biol.* 276, 391–404.
- Porse, B.T., Cundliffe, E., and Garrett, R.A. (1999). The antibiotic micrococcin acts on protein L11 at the ribosomal GTPase centre. *J. Mol. Biol.* 287, 33–45.
- Price, S.R., Ito, N., Oubridge, C., Avis, J.M., and Nagai, K. (1995). Crystallisation of RNA-protein complexes. I. Methods for the large-scale preparation of RNA suitable for crystallographic studies. *J. Mol. Biol.* 249, 398–408.
- Quigley, G.J., and Rich, A. (1976). Structural domains of transfer RNA molecules. *Science* 194, 796–806.
- Ramakrishnan, V., and Biou, V. (1997). Treatment of multiwavelength anomalous diffraction data as a special case of multiple isomorphous replacement. *Methods Enzymol.* 276, 538–557.
- Ramakrishnan, V., and White, S.W. (1998). Ribosomal protein structures: insights into the architecture, machinery and evolution of the ribosome. *Trends Biochem. Sci.* 23, 208–212.
- Ramakrishnan, V., Finch, J.T., Graziano, V., Lee, P.L., and Sweet, R.M. (1993). Crystal structure of globular domain of histone H5 and its implications for nucleosome binding. *Nature* 362, 219–223.
- Rosendahl, G., and Douthwaite, S. (1993). Ribosomal proteins L11 and L10(L12)4 and the antibiotic thiostrepton interact with overlapping regions of the 23 S rRNA backbone in the ribosomal GTPase centre. *J. Mol. Biol.* 234, 1013–1020.
- Rosendahl, G., and Douthwaite, S. (1994). The antibiotics micrococcin and thiostrepton interact directly with 23S rRNA nucleotides 1067A and 1095A. *Nucleic Acids Res.* 22, 357–363.
- Schmidt, F.J., Thompson, J., Lee, K., Dijk, J., and Cundliffe, E. (1981). The binding site for ribosomal protein L11 within 23 S ribosomal RNA of *Escherichia coli*. *J. Biol. Chem.* 256, 12301–12305.
- Sopori, M.L., and Lengyel, P. (1972). Components of the 50S ribosomal subunit involved in GTP cleavage. *Biochem. Biophys. Res. Commun.* 46, 238–244.
- Spahn, C.M., and Nierhaus, K.H. (1998). Models of the elongation cycle: an evaluation. *Biol. Chem.* 379, 753–772.
- Stöffler, G., Cundliffe, E., Stöffler-Meilicke, M., and Dabbs, E.R. (1980). Mutants of *Escherichia coli* lacking ribosomal protein L11. *J. Biol. Chem.* 255, 10517–10522.
- Studier, F.W., Rosenberg, A.H., Dunn, J.J., and Dubendorff, J.W. (1990). Use of T7 RNA polymerase to direct expression of cloned genes. *Methods Enzymol.* 185, 61–89.
- Szewczak, A.A., Moore, P.B., Chang, Y.L., and Wool, I.G. (1993). The conformation of the sarcin/ricin loop from 28S ribosomal RNA. *Proc. Natl. Acad. Sci. USA* 90, 9581–9585.
- Terwilliger, T., and Berendzen, J. (1999). Automated MAD and MIR structure determination. *Acta Crystallogr. D* 55, 849–861.
- Thompson, J., Cundliffe, E., and Stark, M. (1979). Binding of thiostrepton to a complex of 23-S rRNA with ribosomal protein L11. *Eur. J. Biochem.* 98, 261–265.
- Thompson, J., Schmidt, F., and Cundliffe, E. (1982). Site of action of a ribosomal RNA methylase conferring resistance to thiostrepton. *J. Biol. Chem.* 257, 7915–7917.
- Wang, Y.X., Lu, M., and Draper, D.E. (1993). Specific ammonium ion requirement for functional ribosomal RNA tertiary structure. *Biochemistry* 32, 12279–12282.
- Wilson, K.S., and Noller, H.F. (1998a). Mapping the position of translational elongation factor EF-G in the ribosome by directed hydroxyl radical probing. *Cell* 92, 131–139.
- Wilson, K.S., and Noller, H.F. (1998b). Molecular movement inside the translational engine. *Cell* 92, 337–349.
- Wimberly, B. (1994). A common RNA loop motif as a docking module and its function in the hammerhead ribozyme. *Nat. Struct. Biol.* 1, 820–827.
- Wimberly, B., Varani, G., and Tinoco, I., Jr. (1993). The conformation of loop E of eukaryotic 5S ribosomal RNA. *Biochemistry* 32, 1078–1087.
- Wimberly, B.T., White, S.W., and Ramakrishnan, V. (1997). The structure of ribosomal protein S7 at 1.9 Å resolution reveals a beta-hairpin motif that binds double-stranded nucleic acids. *Structure* 5, 1187–1198.
- Xing, Y., and Draper, D.E. (1995). Stabilization of a ribosomal RNA tertiary structure by ribosomal protein L11. *J. Mol. Biol.* 249, 319–331.
- Xing, Y., and Draper, D.E. (1996). Cooperative interactions of RNA and thiostrepton antibiotic with two domains of ribosomal protein L11. *Biochemistry* 35, 1581–1588.
- Xing, Y., Guha Thakurta, D., and Draper, D.E. (1997). The RNA binding domain of ribosomal protein L11 is structurally similar to homeodomains. *Nat. Struct. Biol.* 4, 24–27.